J Appl Electrochem (2008) 38:1727–1734
DOI 10.1007/s10800-008-9624-1

ORIGINAL PAPER

Control of composition and size for Pd–Ni alloy nanowires electrodeposited on highly oriented pyrolytic graphite

Weiwei Si · Gang Yu · Yuejun Ouyang · Lili Tang · Xiaomei He · Bonian Hu

Received: 12 January 2008 / Accepted: 13 June 2008 / Published online: 3 July 2008

Abstract In order to fabricate effective Pd–Ni alloy nanowire arrays with given compositions and size, the process of nucleation and growth and the dependence of alloy composition on deposition potential were investigated. The results reveal that the compositions and sizes of Pd–Ni alloy nanowires can be controlled within a desired range through adjusting suitable nucleation and growth potentials as well as the time. The Ni content in the alloy nanowires was found to vary from 6 to 28% when the deposition potential was changed from −0.3 to −1.9 V. A growth potential of −0.35 to − 0.50 V was applied to fabricate Pd–Ni alloy nanowires with 8–15% Ni content. Continuous and parallel nanowire arrays can be successfully fabricated when nucleation is performed at a potential of −1.2 V for 50 ms with further growth at −0.45 V for 800 s. Pd–Ni crystal phases exist in the alloy structure forms of ⟨111⟩, ⟨200⟩, ⟨220⟩, ⟨311⟩. The nanowires have an average diameter of 150 nm and a length of 100–450 μm.

Keywords Pd–Ni alloy · Nanowires · Composition control · Size control · Highly oriented pyrolytic graphite

W. Si · G. Yu (✉) · L. Tang
State Key Laboratory of Chemo/Biosensing and Chemometrics, College of Chemistry and Chemical Engineering, Hunan University, Changsha 410082, China
e-mail: yuganghnu@163.com

Y. Ouyang
Department of Chemistry and Chemical Engineering, Huaihua College, Huaihua 418008, China

X. He · B. Hu
Department of Chemistry and Chemical Engineering, Hunan Institute of Technology, Hengyang 421002, China

Abbreviations

HOPG	Highly oriented pyrolytic graphite
SED	Step edge decoration
ESED	Electrochemical step-edge decoration
AAO	Anodic aluminum oxide
SEM	Scanning electron microscope
EDX	Energy-dispersive X-ray
XRD	X-ray diffraction
SCE	Saturated calomel electrode
CV	Cyclic voltammogram

1 Introduction

Nanowires are advanced materials of increasing fundamental and technological interest. They have the potential for miniaturizing electronic devices far more than conventional semiconductor technology [1–3]. Various lithographic and non-lithographic [4, 5] techniques are available for nanowire fabrication. One non-lithographic technique for nanowire fabrication is template based manufacturing [6, 7]. This method is based on the synthesis of the desired material within the pores or edges of the template and is accomplished by electrochemical reduction of the appropriate metal ions into the pores or edges.

Nanowires can be obtained by selectively electrodepositing metals or conductive metal oxides at the step edges on an HOPG (Highly Oriented Pyrolytic Graphite) surface [8, 9]. The technique of using step edges as a template to synthesize nanowires, sometimes called “step edge decoration (SED)”, has been known for many years [10–13]. A new development in the SED technique was electrochemical step-edge decoration (ESED). Since nanowires were formed for the first time by the ESED

method, it has become a well-established route for preparing nanowires. As early as 1993, Kern and co-workers [14] studied the growth of one-dimensional Cu on Pd (110). Mukhopadhyay and Freyland [15] electrodeposited Ti nanowires on HOPG at room temperature by ESED. Chains of Ag nanoparticles were synthesized on HOPG with ESED by Francis et al. [16]. Walter et al. [17] demonstrated that ESED can be used to prepare metal nanowires by reducing their metal oxides with diameter adjustability, excellent dimensional uniformity, strength, and lengths of more than 500 μm. Thompson et al. [18] showed that kinetically controlled electro-oxidation can be coupled with the ESED method to prepare antimony, gold and Bi_2Te_3 nanowires with diameters in the range from 20 to 50 nm.

In many applications, the properties of alloys are very important. Recently, Yun and co-workers [19] demonstrated the preparation of $Fe_{0.39}Co_{0.61}$ alloy nanowire arrays by electrodeposition of Fe^{2+} and Co^{2+} into the pores of an AAO (anodic aluminum oxide) template in a mixture solution. The alloy nanowires were shown to greatly improve the coercivety and squareness of the materials. Hughes and Schubert [20] found that a hydrogen sensor based on a Pd–Ni alloy film with Ni content of 8–15 wt.% had rapid response and high reversibility at room temperature. The sensor also showed resistance to poisoning by H_2S. Therefore, Pd–Ni alloy nanowires used for hydrogen sensors can overcome many disadvantages of pure palladium nanowires, which are poisoned easily by exposure to reactive species [21] and easily produce hydrogen bubbles in high concentrations of hydrogen [7, 22].

In our previous work the basic electrolyte composition was established. Pd–Ni alloy nanowires on HOPG were successfully synthesized by ESED [23–25]. However, the alloy composition and sizes were uncertain. The alloy nanowires produced were usually coarse and discontinuous in most situations. Therefore, our work focuses on the fabrication of longer and thinner nanowire arrays for effective connection between the two electrodes for application of hydrogen sensing materials. The relative theories and effective methods of the fabrication process need to be further discussed. The dependence of alloy composition on potential and control methods of alloy nanowire compositions and sizes are described in the present paper.

2 Experimental

2.1 Electrolyte

An aqueous solution composed of 70 mM $Pd(NH_3)_4Cl_2$, 30 mM $NiSO_4$, and 0.2 M NH_4Cl was used as electrolyte for deposition of the Pd–Ni alloy. All chemicals were of analytical reagent purity. The pH value of the Pd–Ni alloy electrolyte was adjusted to 8.5 with $NH_3 \cdot H_2O$. The blank electrolyte was a pH 8.5 solution of 0.2 M $NH_4Cl + NH_3 \cdot H_2O$ without $Pd(NH_3)_4Cl_2$ and $NiSO_4$. The electrolyte was prepared using double distilled water. In order to eliminate oxygen from the electrolyte, it was bubbled with argon gas (99.995%) for 15 min prior to use.

2.2 Cell and electrodes

All electrodeposition experiments were carried out in a glass, one-compartment, three-electrode cell. The HOPG (5 × 3 × 1 mm^3, ZYA grade) was masked by epoxy resins and a 5 × 3 mm^2 area was exposed as working electrode. Before each experiment, the HOPG electrode was freshly cleaved with adhesive tape. Platinum foil (about 2 cm^2) was employed as the counter electrode and the reference electrode used was a saturated calomel electrode (SCE). The potential values are vs. SCE in the whole paper.

2.3 Electrodeposition

Alloy nanowires were prepared by applying three voltage pulses in succession: an oxidation pulse of +0.8 to + 1.0 V for 5 s, a negative reducing nucleation pulse for 1–50 ms and a growth pulse in a duration of several minutes. The potential were controlled by a computer-operated electrochemical work station (CHI660B).

2.4 SEM, EDX and XRD characterization

After alloy nanowire arrays were fabricated, the HOPG electrode was removed from the electrolyte and rinsed with double distilled water. The morphology and the composition of the alloy nanowire arrays were analyzed by a JSM-5600 LV scanning electron microscope (SEM) equipped with a Noran Vantage 4105 energy-dispersive X-ray (EDX) elemental analyzer. The crystal structures of the alloy nanowires were characterized by X-ray diffraction (XRD, Rigaku model D/max 2400; Cu Kα radiation, λ = 0.154056 nm).

3 Results and discussion

3.1 Pd–Ni codeposition and analysis of compositions and structures

3.1.1 Cyclic voltammogram of Pd–Ni alloy electrolyte

Cyclic voltammograms (CV) in the electrolyte (see solid curve) and in the blank solution (see dash curve) described in Sect. 2 are shown in Fig. 1. The two curves both display

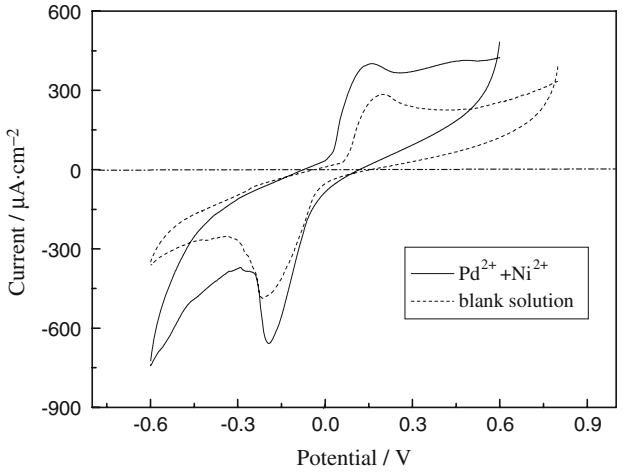

Fig. 1 Cyclic voltammogram of the HOPG electrode in the electrolyte and blank solution

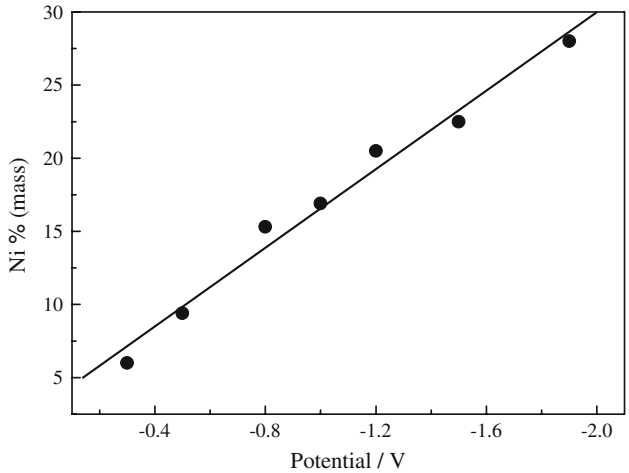

Fig. 2 The dependence of Ni content in the Pd–Ni alloy on the deposition potentials

a cathodic peak of evolving H_2 at −0.2 V. The reduction current decreases between −0.2 and −0.3 V since the H_2 bubbles adsorbed on HOPG decrease the reaction area of the electrode. The decrease in electrode area leads to lower reaction current. Thus the height of the cathodic peak is depressed after −0.21 V. The cathodic current peak is located in the valley at about −0.3 V as the least reaction area appears on the electrode saturated with H_2 bubbles. It is important to note that the change in electrode area can alter the reaction current owing to coverage by gas bubbles, but it cannot shift the position of the peak potential.

The cathodic current of solid curve in Fig. 1 is always lower than that of the dashed curve between 0 and −0.6 V. This indicates that the codeposition of Pd–Ni and the evolution of hydrogen occur simultaneously from −0.2 to −0.6 V. The deposited Palladium can further catalyze the evolution of hydrogen. A further experiment proved that alloy nanoparticles were not observed by SEM after electrodepositing for 10 h at a constant −0.2 V, but they can be seen at constant −0.3 V. It shows that the formation of hydrogen bubbles is initiated from −0.2 to −0.3 V, but is accelerated from −0.3 to −0.6 V after codeposition of Pd–Ni alloy, as shown in Fig. 1. The anodic peaks of the two curves in Fig. 1 appear since hydrogen or both hydrogen and metal nickel are oxidized at about +0.15 to + 0.2 V in the blank solution or the electrolyte, respectively.

Moreover, the CV experiment suggests that alloy nanowires should be fabricated under a deposition potential that is more negative than −0.3 V.

3.1.2 Composition control of Pd–Ni alloy

The composition of Pd–Ni alloy was investigated by EDX. The alloy composition depends both on electrolyte composition and on electrodeposition conditions. The effect of palladium and nickel ion concentration ratio on the composition of Pd–Ni alloy nanowires were systematically investigated in our previous work [25, 26]. The dependence of Ni content in the alloy on deposition potential is shown in Fig. 2.

The Ni content increases linearly with potential from −0.3 to −1.9 V. The current increases when the potential moves negatively. It is propitious to raise the deposition rate of the more negative metal and to increase the ratio of nickel in the alloy. The Ni content can be controlled to 8–15% when −0.35 to −0.88 V is applied. Alloy with this nickel content is a good material which can resist hydrogen damage [20]. The alloy composition is completely controlled by adjusting the deposition potential. Obviously, the various compositions in the inner and outer layer of nanowires are formed when two different potentials are used for nucleation and growth.

3.1.3 Phase structure of the Pd–Ni deposits

Electrodeposition was operated based on the experimental procedures in Sect. 2. At −0.7 V for 0.5 h, a Pd–Ni alloy with 13% Ni content was obtained. The phase structure of the Pd–Ni alloy was investigated using XRD as shown in Fig. 3 which displays four alloy peaks. The crystal lattice indexes of these diffraction peaks correspond to interplaner spacing (d) 2.2106, 1.9123, 1.3492, 1.1558. Diffraction data of single palladium and single nickel crystals are listed in Table 1 (source: 1999 JCPDS-International Centre for Diffraction Data, PCPDFWIN v. 2.02). From Table 1, the diffraction peaks of Pd ⟨111⟩ and Ni ⟨111⟩ correspond to interplaner spacing (d) 2.2326 and 2.2034, respectively. It is apparent that the peak of deposited Pd–Ni is located between Pd ⟨111⟩ and Ni ⟨111⟩. These results strongly indicate that the deposits are alloys of Pd and Ni.

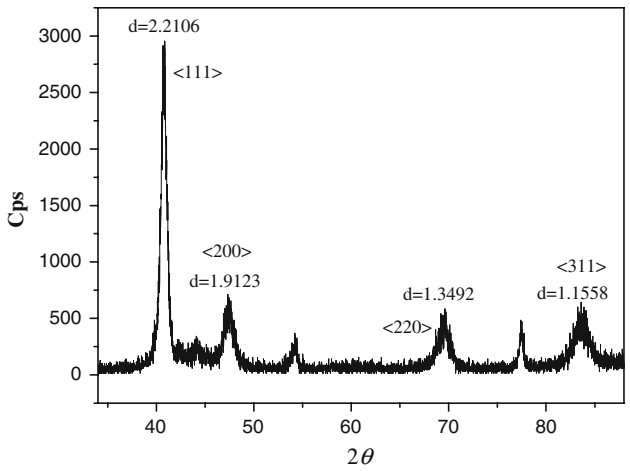

Fig. 3 XRD pattern of Pd–Ni alloy

Table 1 *d* values determined from XRD patterns

Samples	*d* values			
Alloy	2.2106	1.9123	1.3492	1.1558
Pure Pd	2.2326	1.9335	1.3671	1.0624
Pure Ni	2.2034	1.762	1.246	1.1659

3.2 Size control in nucleation and growth processes

3.2.1 Selection of nucleation pulse and growth pulse

If electrodeposition is carried out on an HOPG electrode, there is high selective nuclei density at step edges under the larger overpotentials, but growth occurs on the original nuclei sites without new nuclei formation under lower overpotentials. Three successive pulse potentials of oxidation, nucleation and growth are applied to deposited alloy nanowires based on the experiment procedures described above. Before nanowires are deposited, an oxidation pulse of +0.8 V for 5 s was exerted for optimizing step edges on the surface of HOPG.

−1.2 to −1.9 V was chosen as the nucleation potential in order to obtain enough nuclei density for forming nanowires [25]. If the nucleation potential is more negative than −1.9 V, dense nanoparticles are scattered on HOPG terraces without selectivity, which goes against preparing separate nanowire arrays at step edges. However, if the nucleation potential is more positive than −1.2 V, continuous nanowires cannot easily be formed. Therefore, the optimum range of nucleation potential is from −1.2 to −1.9 V. More continuous nanowires are obtained by selecting an appropriate nucleation potential.

Under the nucleation potential of −1.2 to −1.9 V, water is decomposed to produce H_2 on the cathode but the nucleation is instantaneously completed and it lasts for only 50 ms. The hydrogen bubbles formed need longer time, while the metal nuclei are formed faster than hydrogen gas. How does the hydrogen evolution affect the formation of metal nuclei? The mechanism is not clear at present. This work needs further investigation through experiments. We think that atomic hydrogen evolution will permeate into crystal grains of Pd–Ni alloy to form a metal hydride. Nano-pinholes in the nanowires will be formed under the more negative growth potential for a long time.

In the growth phase, the coarsening rate of nanowires is much lower than that in the nucleation phase. The gaps between nanoparticles of the chains formed at the nucleation stage are mainly filled in the growth stage. It is propitious to produce a Pd–Ni alloy with 8–15% Ni content on the surface layer of nanowires when the deposition potential of −0.35 to −0.88 V is used as growth potential pulse. The nanowire arrays cannot be formed if an unsuitable potential is selected and more nanoparticles are produced on the HOPG electrode surface. −0.35 to −0.50 V was established as growth potential of smooth nanowires.

3.2.2 Size change in nucleation and growth process

After nucleation is instantaneously completed, the diameters of the Pd–Ni alloy nanowires can be controlled by changing the deposition time, t_{dep}. If the growth current is a steady-state current and is associated purely with the deposition of hemi-cylindrical nanowires, the time-dependent radius of these structures, $r(t)$, is given by [27].

$$r(t) = \sqrt{\frac{2i_{dep}t_{dep}V_m}{\pi zFl}} \quad (1)$$

In Eq. 1, i_{dep} is the steady-state deposition current density, t_{dep} is the total deposition duration, V_m is the molar volume of the deposited material, z is the number of electrons transferred for the deposition of each metal atom, and l is the total length of nanowires on the HOPG. It has been proven that the diameters of nanowires such as MoO_2 [28], copper, silver, nickel, and gold [4] obey this law. However, Eq. 1 is found to be unsuitable for the growth of Pd–Ni nanowires.

The process of alloy nanowire expansion should include the primary formation of nanowires after instant nucleation in the nucleation pulse and the development in the growth pulse. Figure 4 reveals the dependence of the diameter of Pd–Ni alloy nanowires on nucleation time (t_{nucl}) at −1.9 V nucleation potential from 1 to 50 ms without a growth pulse. When nanowire arrays were fabricated with a −1.9 V nucleation pulse for 4 ms without growth pulse, parallel continuous nanowire arrays with an average diameter of about 70 nm were obtained. When the nucleation time lasted 40 ms, the average diameter increased to 125 nm.

The diameter reached 150 nm when a −1.9 V 50 ms nucleation pulse was applied. It is apparent that nuclei are instantly completed and are concomitant with growing simultaneously in the nucleation phase.

By regression treatment of the experimental data in Fig. 4, the relation between r and t can be expressed as

$$r(t) \propto t^{0.34} \tag{2}$$

The dependence of the diameter increment developed in the growth phase on the growth time (t_{growth}) is shown in Fig. 5. The increments varied with growth time are from 0 to 170 nm by growth pulse of −0.45 V for 0–1,500 s.

The growth equation for Pd–Ni alloy nanowires in the growth phase is found to be

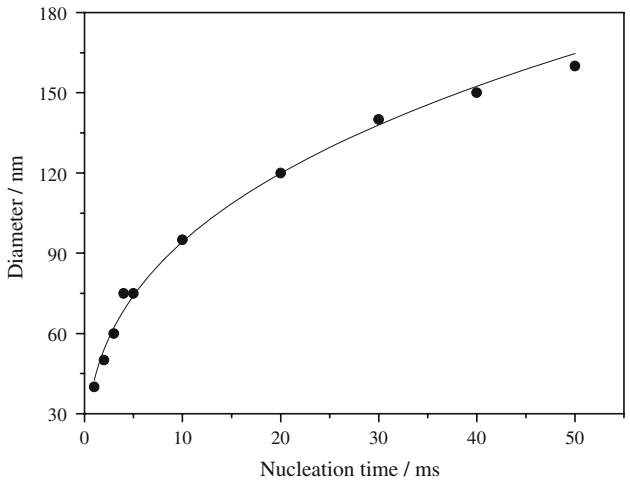

Fig. 4 The dependence of diameter of nanowires on nucleation time by nucleation at −1.9 V

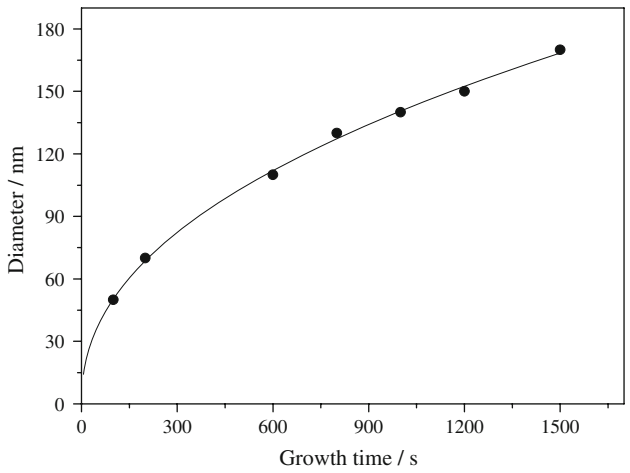

Fig. 5 The dependence of diameter increment of nanowires on growth time at the growth potential of −0.45 V

$$r(t) \propto t^{0.44} \tag{3}$$

Walter and co-workers [24] reported that the growth for a Pd nanowire has the relation $r(t) \propto t^{\frac{1}{3}}$. For Ni, it is $r(t) \propto t^{\frac{1}{2}}$ [24]. Therefore it is expected that the diameter growth equation for a Pd–Ni nanowire should be $r(t) \propto t^{\frac{1}{3}-\frac{1}{2}}$, i.e. $r(t) \propto t^{0.33-0.50}$. The experimental value is $r(t) \propto t^{0.34-0.44}$. The experimental time exponents are between those from growth equations of single palladium and single nickel.

The diameter increment for nanowires formed in the nucleation and growth pulses can be expressed by Eqs. 4 and 5, respectively:

$$\Delta d_{\text{nucl}} = \text{A} t_{\text{nucl}}^{0.34} \tag{4}$$

$$\Delta d_{\text{growth}} = \text{B} t_{\text{growth}}^{0.44} \tag{5}$$

Differentiating Eqs. 4 and 5 gives

$$\frac{\text{d}(\Delta\, d_{\text{nucl}}\,)}{\text{d}t_{\text{nucl}}} = \text{A}\frac{1}{0.34} t_{\text{nucl}}^{1-0.34} = \text{C} t_{\text{nucl}}^{0.66} \tag{6}$$

$$\frac{\text{d}(\Delta\, d_{\text{growth}}\,)}{\text{d}t_{\text{growth}}} = \text{B}\frac{1}{0.44} t_{\text{growth}}^{1-0.44} = \text{D} t_{\text{growth}}^{0.56} \tag{7}$$

In the above Eqs. 4–7, A, B, C and D are independent of time. Based on Eqs. 6 and 7 for the rates of diameter increase in the nucleation and growth phase, it is evident that the deposition rate of nanowires in the nucleation stage is much faster than that in the growth stage. Therefore, the effect of nucleation pulse on the diameter of nanowires is much greater than that of the growth stage.

Nucleation is a very important stage in the successful synthesis of Pd–Ni alloy nanowire arrays. In this stage, nanoparticle nuclei are formed instantly and growth of the nucleation sites leads to rapidly expanding nanoparticles diameters under a large overpotential. Even when the nucleation time is changed by a small amount the diameter will be greatly affected. Therefore, size control of the nanowire diameter needs to be precisely controlled through the nucleation potential and time. However, satisfactory nanowires with a desired size are not obtained by only controlling nucleation without controlling the growth process. Smaller growth overpotential leads to lower coarsening rate of nanowires. Smooth nanowires are formed at a slower growth rate. So sizes, compositions and morphologies of nanowires can be changed by adjusting both the potential and time of nucleation and growth.

Nanowires with different compositions are prepared due to the big difference of the nucleation potential and the growth potential. There is higher Ni content inside nanowires and lower Ni content outside the nanowires. The composition of the surface layer on the nanowires significantly affects hydrogen adsorption kinetics. It is propitious to obtain the nanowire outside layers with the given composition by precise control of growth potential.

3.3 Probability of successful nanowire formation

The effect of nucleation time on Pd–Ni alloy nuclei density at step edges of HOPG at the nucleation potential of −1.9 V is shown in Fig. 6.

The density of nanoparticles at step edges was proportional to the nucleation time between 1 and 20 ms, but the density of nuclei was nearly independent of the nucleation time beyond 20 ms. Therefore, the successful probability for the fabrication of continuous nanowires will decrease if nucleation lasts for less than 20 ms. Enough nanoparticles to form nanowires were not obtained at step edges until the nucleation time was greater than 20 ms.

Our experiments have validated that there is a higher successful probability to form nanowires with −1.9 V nucleation than that with −1.2 V nucleation if the same nucleation time is used, but unduly coarse nanowires are obtained at −1.9 V. It is indispensable that more continuous nanowire arrays are obtained by nucleation at appropriate lower potential and then through further growth.

The 70 nm nanowires can be obtained under the condition of −1.2 V nucleation for 50 ms without growth, as shown in Fig. 7a, but the diameter of nanowires reaches about 150 nm with further growth at −0.45 V for 800 s (see Fig. 7b). The nanoparticles distributed on terraces of HOPG in Fig. 7a are denser than those in Fig. 7b, which illustrates that growth makes nanoparticles move and couple. Slow growth is an effective means for eliminating interparticle diffusion coupling because the radii of the depletion layer adjacent to each Pd–Ni alloy nanoparticle are reduced as the growth rate is decreased. Equalizing the growth rates of Pd–Ni alloy nanoparticles is to generate convective mixing of the electrolyte in the vicinity of each alloy particle [27].

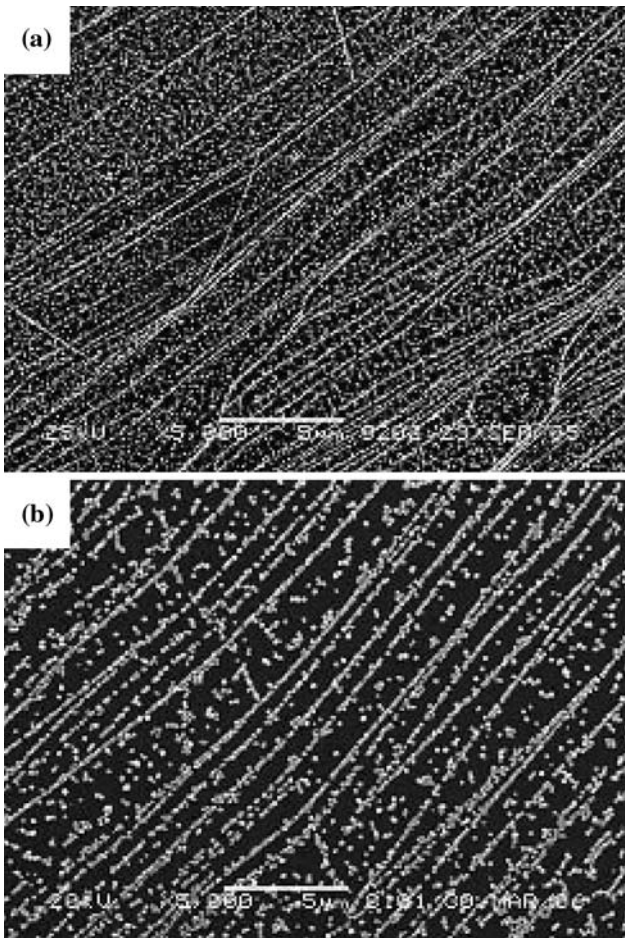

Fig. 7 (**a**) SEM images of the nanowires obtained by only nucleation at −1.2 V for 50 ms; (**b**) SEM of the nanowires obtained by nucleation at −1.2 V for 50 ms with further growth at −0.45 V for 800 s

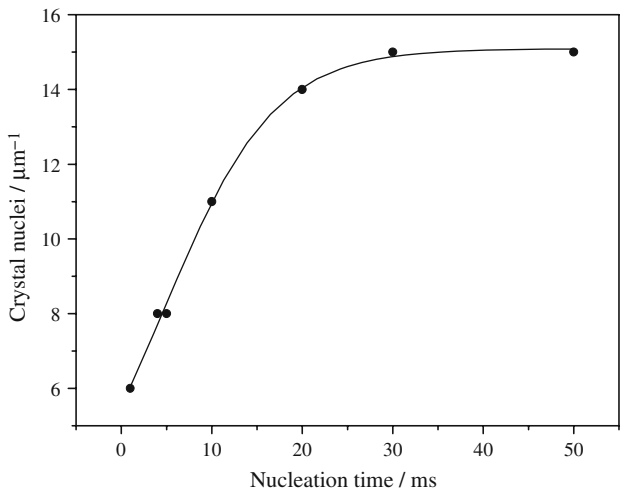

Fig. 6 The dependence of the density of crystal nuclei at step edges on nucleation time at the nucleation potential of −1.9 V without growth

Beaded chains of Pd–Ni alloy nanoparticles are formed by nucleation at −1.2 V for 100 ms and by growth at −0.3 V for 30 min, which show that the gaps between nanoparticles cannot be completely filled to form smooth nanowire arrays under −0.3 V growth potential, as shown in Fig. 8.

When the nucleation potential was increased to −1.9 V for 50 ms and the growth potential was changed to −0.45 V for 1,500 s, thick alloy nanowires of diameter of 300–500 nm are formed, as shown in Fig. 9. The gaps between nanoparticles can be completely filled to form smooth nanowire arrays under −0.45 V growth potential, but the nanowires are not elegant.

A clearer SEM image of elegant alloy nanowire arrays fabricated by nucleation at −1.2 V for 50 ms and by growth at −0.45 V for 800 s is shown in Fig. 10. It shows that smooth nanowires have an average diameter of about

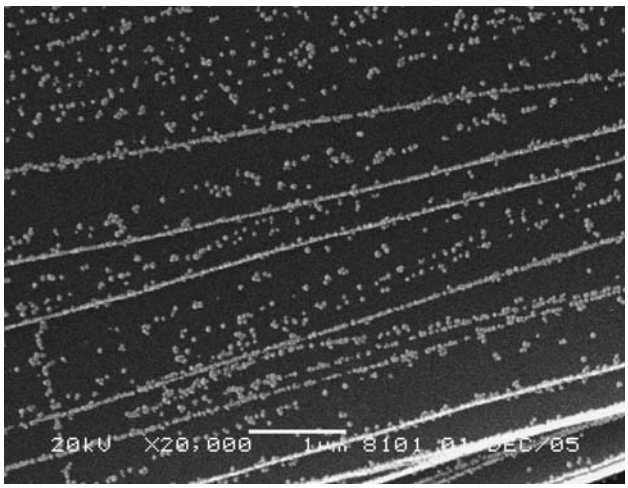

Fig. 8 SEM image of the beaded chains obtained by nucleation at −1.2 V for 100 ms with further growth at −0.3 V for 30 min

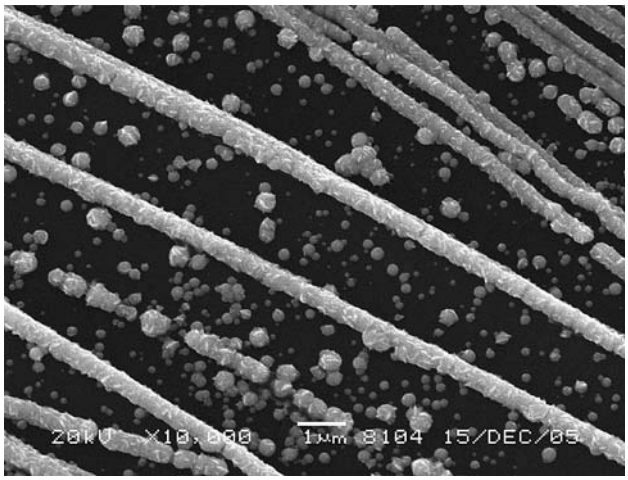

Fig. 9 SEM image of the smooth thick nanowires obtained by nucleation at −1.9 V for 50 ms with further growth at −0.45 V for 1,500 s

150 nm. The longest nanowires reach up to 450 μm through mobile measurement using SEM. From Figs. 8 to 10 the suitable growth potential selected is a more important parameter to smooth nanowires.

Nanowire length mainly depends on the state of the HOPG surface. If the steps on HOPG are parallel and sufficiently long, parallel and long nanowires will be fabricated. Curved or discontinuous nanowires will be produced on curved or broken step edges on HOPG.

4 Conclusion

1. The various compositions in the inner and outer layer of nanowires were formed by using two different potentials for nucleation and growth. The Pd–Ni alloy with Ni content of 8–15% could be fabricated between −0.35 and −0.88 V. This alloy exists in main forms of ⟨111⟩ crystal phase structure. The growth potential of −0.35 to − 0.50 V was applied to fabricate Pd–Ni alloy nanowires with the required composition and good morphologies.
2. Sizes, compositions and morphologies of nanowires can be changed by adjusting both the potential and time of nucleation and growth. The deposition rate of nanowires in the nucleation stage is much faster than that in the growth stage. The size control of nanowire diameters relies on precisely adjusting nucleation potential and time. Growth at lower overpotential can smooth the nanowire surface and control the surface composition of the nanowires.
3. High success probability for the fabrication of continuous and elaborate nanowires can be obtained through nucleating at −1.2 V for over 20 ms and then growing at a suitable potential between −0.35 and −0.50 V.

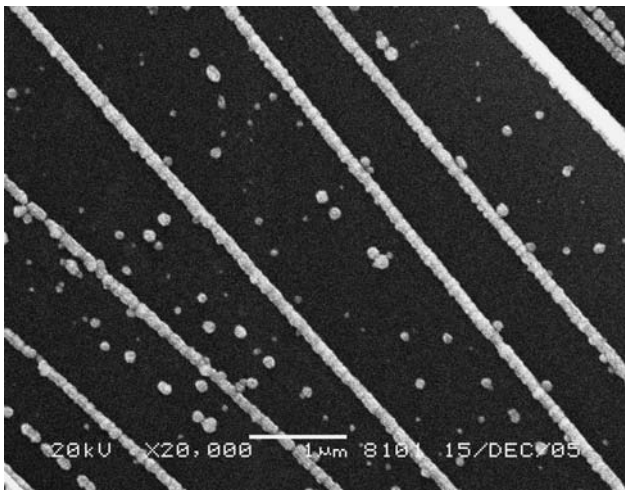

Fig. 10 SEM image of Pd–Ni alloy nanowire arrays formed by nucleation at −1.2 V for 50 ms with further growth at −0.45 V for 800 s

Acknowledgments This work was supported by the National Natural Science Foundation of China (Grant No. 20373015) and Hunan Education Office (Grant No. 04C033).

References

1. Roman LS, Berggren M, Inganas O (1999) Appl Phys Lett 75:3557
2. Xia Y, Yang P, Sun Y, Wu Y et al (2003) Adv Mater 15:353
3. Li C, Zhang D, Liu X et al (2003) Appl Phys Lett 82:645
4. Walter EC, Murray BJ, Favier F et al (2002) J Phys Chem B 106:11407
5. Zach MP, Ng KH, Penner RM (2000) Science 290:2120
6. Martin CR (1996) Chem Mater 8:1739
7. Faver F, Walter E, Zach M et al (2001) Science 293:2227

8. Menke EJ, Li Q, Penner RM (2004) Nano Lett 4:2009
9. Li Q, Olson JB, Penner RM (2004) Chem Mater 16:3402
10. Jung T, Schlittler R, Gimzewski JK et al (1995) Appl Phys A 61:467
11. Gambardella P, Blanc M, Brune H et al (2000) Appl Phys B 61:2254
12. Dekoster J, Degroote B, Pattyn H et al (1999) Phys Rev Lett 75:938
13. Morin S, Lachenwitzer A, Magnussen OM et al (1999) Phys Rev Lett 83:5066
14. Roder H, Hahn E, Brtune H et al (1993) Nature 366:141
15. Mukhopadhyay I, Freyland W (2003) Langmuir 19:1951
16. Francis GM, Kuipers L, Cleaver JRA et al (1996) J Appl Phys 79:2942
17. Walter EC, Zach MP, Favier F et al (2003) Chemphyschem 4:131
18. Thompson MA, Menke EJ, Martens CC et al (2006) J Phys Chem B 110:36
19. Guo Y, Qin DH et al (2003) Appl Surf Sci 218:107
20. Hughes RC, Schubert WK (1992) J Appl Phys 71:542
21. Christofieds C, Mandelis A (1990) J Appl Phys 68:R1
22. Scharnagl K, Eriksson M, Karthigeyan A et al (2001) Sens Actuators B 78:138
23. Xiao YK, Yuan J, Hu BN et al (2004) J Hunan Univ 31:5
24. Yuan J, Xiao YK, Yu G et al (2005) Acta Phys Chem Sin 21:602
25. Xiao YK, Yu G, Yuan J et al (2006) Electrochim Acta 51:4218
26. Yuan J, Xiao YK, Yu G et al (2004) Electroplat Pollut Control 24:14
27. Penner RM (2002) J Phys Chem B 106:3339
28. Zach MP, Inazu K, Ng KH et al (2002) Chem Mater 14:3206